CHAPTER-5

RESULT AND DISCUSSION: SiC PARTICULATE REINFORCED METAL MATRIX COMPOSITES

RESULT AND DISCUSSION: SiC PARTICULATES REINFORCED METAL MATRIX COMPOSITES

This chapter deals with the microstructural, mechanical and tribological properties of AZ91 magnesium alloy and its composite reinforced by different weight percent of SiC (average particle size around 40 microns) particulates. The results have been discussed to develop a coherent understanding of the different properties of the composites.

5.1. Introduction

Magnesium-based materials are becoming the essential material for structural application worldwide due to their weight reduction capabilities. It is used extensively in the automobile and aerospace industries.

The effect of small variation (3 %, 6 %, 9 % and 12 % by weight) of SiC particles (average size around 40 μm) is used to developed AZ91 magnesium alloy composites. The vacuum assisted stir casting process is employed for the synthesis of composites. This chapter deals with the variation in density with the addition of different weight percentage of SiC in AZ91 magnesium alloy. The microstructural features and X-ray diffraction analysis are conducted to find out the different phases present in the AZ91 alloy and in its composites. The mechanical tests such as hardness, tensile and compressive tests along with SEM factographs of tensile and compressive fracture surfaces are also performed to evaluate the behaviors of these materials. Wear behavior of structural material is one of the crucial parameters for its applicability. It is assumed that the wear properties of composites generally found to be higher than the base alloy.

Therefore, the addition of hard ceramic particles certainly improves the wear properties. Pin on disk dry sliding wear analysis is done to determine the wear behavior of the alloy and also the composites.

5.2. Results and discussion

5.2.1. Density Measurement

The density of the AZ91 alloy and its composites have been experimentally determined using Archimedes principle [207]. The theoretical densities of the magnesium alloy (AZ91) and its composites samples are calculated using the rule-of-mixtures; assuming that there is no Mg/Al/Zn-SiC interfacial reaction. Table 5.1 gives the results of density measurements of monolithic AZ91 and its composites. The measured densities of the composites are very close to that of the theoretical densities. Thus, near-dense and porosity free composites can be consistently produced using the vacuum-assisted stir casting methodology adopted in the current study. However, as the amount of reinforcement increases the porosity is also found to increase slightly. The density values of the composites are in general higher than that of the monolithic alloys.

Further, the density values are found to increase with the increasing weight percentage of SiC particulate, and it is due to the presence of comparatively higher density SiC particulate in magnesium alloy [208]. The porosity also exhibits a gradual increase as the weight percentage of reinforcement's increases in the composite. The increase in porosity in composites is due to increase micro-voids near the vicinity of the large SiC particle. Similar observations are also reported by other authors [130] about magnesium alloy metal matrix composites reinforced with SiC particulates and fabricated through stir casting techniques.

Table 5.1: Density and porosity measurements of AZ91 alloy and its composite (AZ91/SiC)

Materials	**Reinforcements (Wt %)**	**Theoretical Density (g/cm^2)**	**Experimental Density (g/cm^2)**	**Porosity (%)**
AZ91	0	1.8101	1.8005	0.53
AZ91+3 % SiC	3	1.8333	1.8057	1.50
AZ91+6 % SiC	6	1.8559	1.8199	1.94
AZ91+9 % SiC	9	1.8778	1.8322	2.42
AZ91+12 % SiC	12	1.8990	1.8474	2.71

5.2.2. Microstructure Characterization

Microstructural characterization studies were carried out by optical microscopy (OM) and scanning electron microscope (SEM) [209] on the as-cast AZ91 magnesium alloy and SiC particulates reinforced AZ91 magnesium alloy composites, in order to examine the shape and size, and morphological characteristics of grains, presence of porosity, distribution of SiC particulates, and interfacial characteristics of SiC particulates with the AZ91 magnesium alloy matrix [210]. The samples for the microstructural characterization are prepared by cutting, grinding, and polishing on different grit size of the abrasive paper. Microstructural characterization was carried out on the etched AZ91 and AZ91/SiC composites samples using a Leica optical microscope (OM) equipped with Leica application suite and ZEISS scanning electron microscopes (SEM) equipped with energy dispersive spectroscopy (EDS). The ground and polished specimens were used for SEM to investigate reinforcement distribution and interfacial integrity between the reinforcement and matrix alloy. In theory, the homogeneous distribution of reinforcements should be achievable irrespective of the size and amount of the reinforcements. However, at a higher percentage of SiC particulate, some clustering segregation may be possible in the composites.

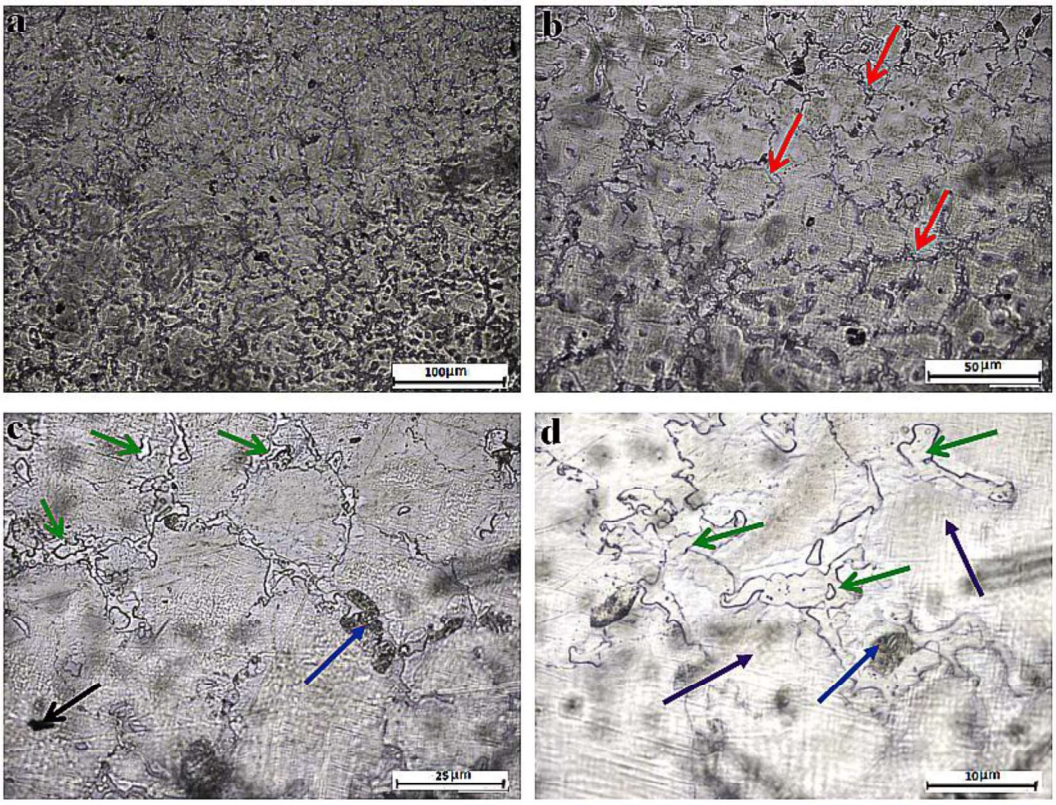

Figure 5.1: Optical Micrograph of AZ91 Magnesium Alloy at different magnifications a) 50X b) 100X c) 200X d)500X

Figure 5.1 shows the optical micrograph of the AZ91 magnesium alloy at different magnifications displaying various phases and the porosity in magnesium alloy marked with different arrows. The black arrow shows the porosity; green arrows show green arrows represent α- phases and β-phases. The β-phases are generally having the composition of Mg_{17} (Al, Zn) $_{12}$. The red arrows represent the grain boundary in AZ91 alloy. Figure 5.2 shows the optical micrograph of the AZ91 magnesium alloy at a different location and 200X magnifications. The bright area in Figure 5.2 shows primary magnesium dendrites (α- phases) which are coexisting with dark inter dendrite precipitate of intermetallic β-phases. The green arrow represents α- phases, β-phases are represented by saffron, and the blue arrow represents β-phases in excess of aluminum. Figure 5.3 shows the optical micrograph of AZ91/SiC composites at different (3 %, 6%, 9%, and 12 %) weight percentage in AZ91.

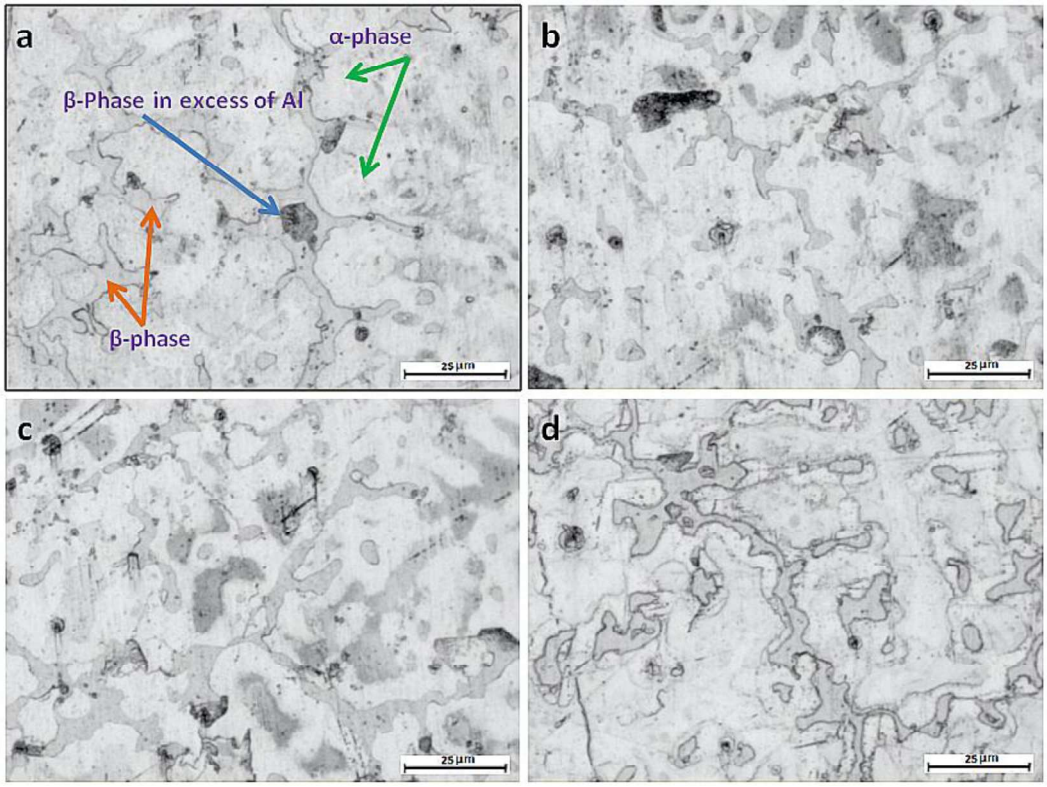

Figure 5.2: Optical Micrograph of AZ91 Magnesium Alloy at different places with magnifications 200X

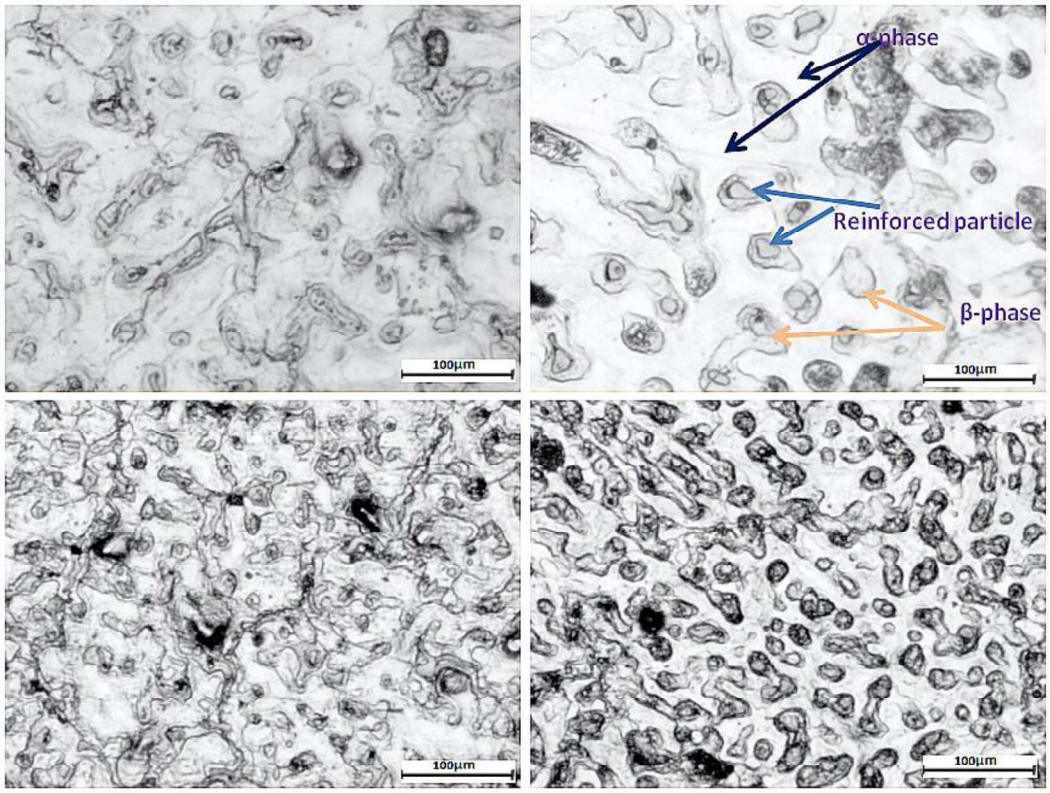

Figure 5.3: Optical Micrograph of AZ91/SiC Magnesium Alloy composite at different weight percentage a) 3 % SiC b) 6% SiC c) 9% SiC d) 12 % SiC

The bright area is found to be dendritic morphology. The grains are refined in the addition of SiC particulate in AZ91 magnesium alloy. Further, on increasing the percentage of SiC particulate, the size of grains becomes finer. The reduction in grain size may be attributed to the nucleation and enhanced recrystallization effect favored by SiC particulates. The hard reinforced particle seems to be embedded in the matrix of the composites. The wettability of the reinforcement is assumed to be good as a reinforced particle are tightly bonded with the matrix materials. The shape and size of the particle are not uniform, so there is a possibility of small porosity in the composite due to the addition of discontinuous reinforcement.

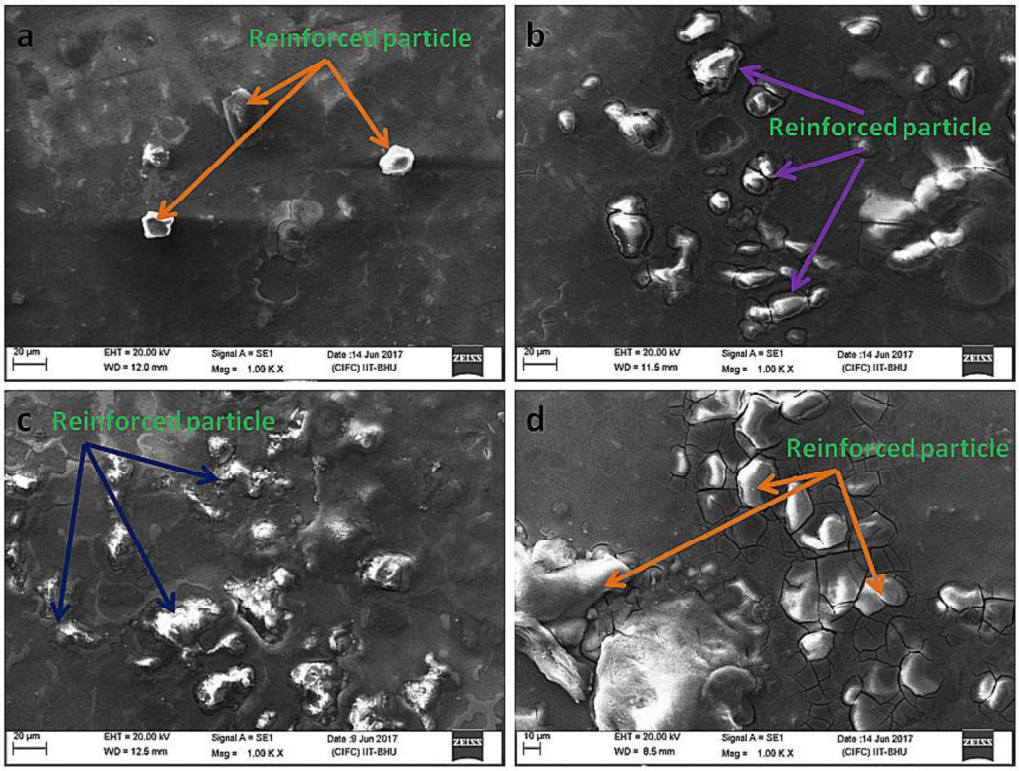

Figure 5.4: SEM micrograph showing distribution of SiC particulate in AZ91 magnesium alloy (a) 3 % SiC (b) 6% SiC (c) 9% SiC (d) 12% SiC

Figure 5.4 shows the SEM micrograph of SiC particulate reinforced composites at a different percentage of SiC particulates. The distribution of SiC particulates in AZ91 magnesium alloy seems to be reasonably uniform, but in some places, the

accumulations of particles have been seen. The accumulated particles of SiC at some places are observed in Figure 5.4, which is marked by the arrow of a different color.

5.2.3. X-ray Diffraction

Figures 4.5 shows the X-ray diffraction analysis results corresponding to magnesium alloy AZ91 and its composites with 3, 6, 9, and 12 weight % reinforced of SiC particulates. The lattice spacing's (d) obtained are matched with that of pure magnesium, SiC_p, and $Mg_{17}Al_{12}$ phases based on the data available in JCPDS/PCPDFwin data. It revealed the presence of the magnesium matrix, the inter-metallic phases $Mg_{17}Al_{12}$, and the reinforcement SiC_p. All the peaks are identified according to the intensity plot of the XRD data. The results, in particular, confirm the absence of MgO, which formation is prevented due to the incorporation of vacuum and argon gas inert atmosphere maintained during the melting and castings.

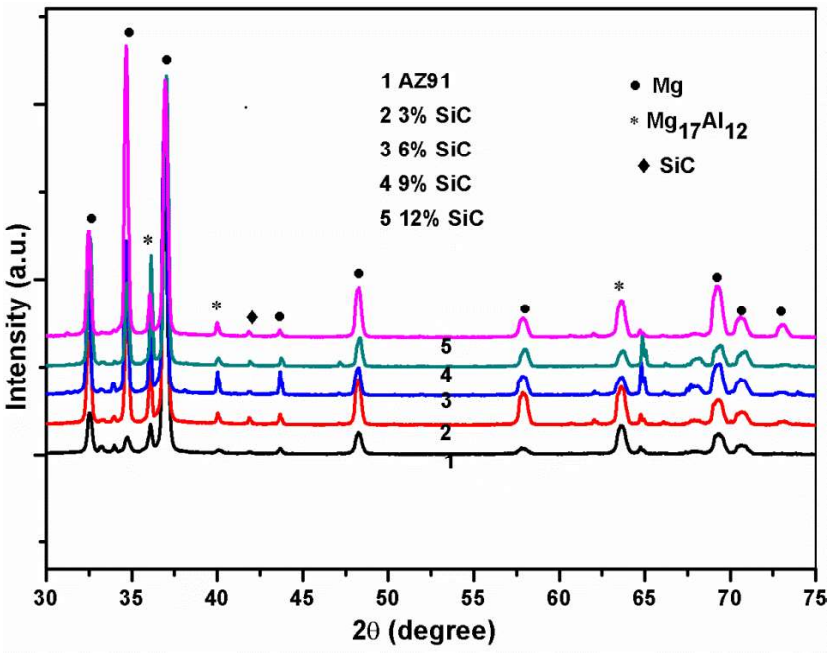

Figure 5.5: X-ray diffraction analysis of magnesium alloy and its composites with different (3%, 6%,9% and 12%) weight percentage

5.2.4. Hardness Test

Vickers microhardness was investigated to understand the effect of the homogeneous distribution of SiC particles within magnesium alloy (AZ91). A rectangular cross-section sample (15 mm x 30 mm) of each fabricated composite has been used to measure the Vickers microhardness. The Vickers microhardness value examined throughout the cross-section at ten different points (at the load of 9.81N) of the AZ91 alloy and its composites reinforced with SiC particulates. There is a slight variation in hardness value at different point of the cross-section of the AZ91 alloy and its composites. It shows fairly uniform distribution of SiC particle within the magnesium alloy matrix. The variation in hardness in AZ91 alloy is due to the presence of hard intermetallic secondary phase in magnesium alloy. The variation in composites is due to the presence of different size of reinforcement as well as slight accumulation of particle at some places. Figure 5.6 shows the variation in microhardness value of magnesium alloy (AZ91) and its composites reinforced with SiC particulate with weight percentage variation (3%, 6%, 9%, and 12%). From Figure 5.6 it was observed that there is an increase in the hardness when the content of reinforcement is increased from 3 to 12 weight percent. The average Vickers microhardness of the magnesium alloy AZ91 and its composites reinforced with SiC particulate are shown in Table 5.2 and Figure 5.7. The hardness value of the composite is increased as the percentage of SiC reinforcement increases. The Vickers hardness value is increased by 32% on the addition of 3% of SiC particulate, and it further increased up to 78% on the addition of 12 % of SiC particulate. The hardness value of the composites with different percentage of SiC (3 %, 6 %, 9 %, and 12%) particulate are found to be higher than magnesium alloy because of the finer grain size and interactive influence of the presence of SiC particulate which restricts the localized matrix deformation during indentation of the composites.

Table 5. 2: Vickers microhardness of magnesium alloy and its composite

Sr. No	Materials	Hardness (HV)
1.	A Z91	60±1.8
2.	3% SiC	79.51±3.4
3.	6% SiC	87.67±4.5
4.	9% SiC	103.45±2.5
5.	12% SiC	107±3

The presence of hard SiC particles will increase the load bearing capacity and also restrict the deformation of the matrix by constraining the dislocation movement. The hardness value of the magnesium alloy composites increases with the increase in the weight percentage of SiC particulate reinforcement.

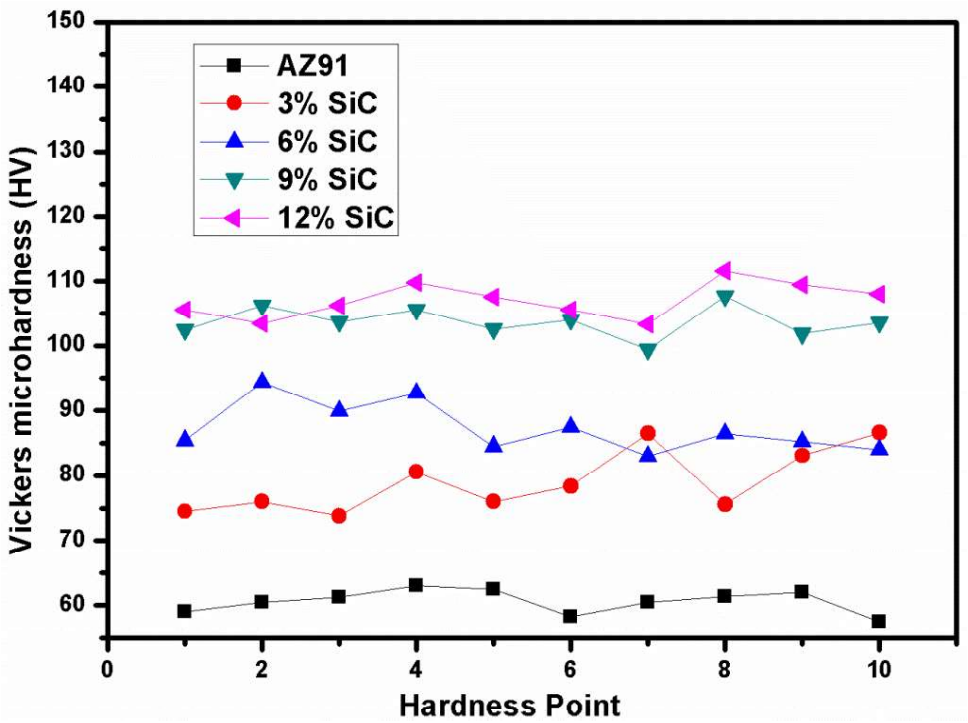

Figure 5. 6: Variation of Vickers microhardness at the load of 9.81N at different location of the alloy and composites with different percentage of SiC particulates

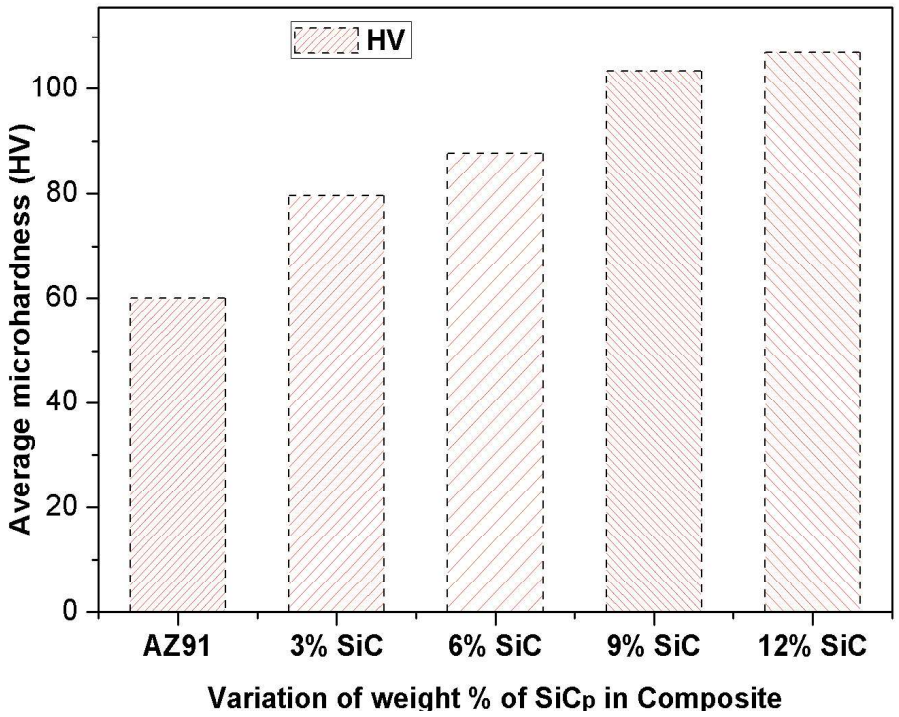

Figure 5. 7: Average Vickers microhardness of alloy and composite with different percentage of SiC particulates at the load of 9.81 N

5.2.5. Tensile Test

The ultimate tensile strength and yield strength of the AZ91 and its composite with a different weight percentage of SiC (3 %, 6 %, 9 %, and 12 %) are given in Table 5.3**.** Figure 5.8 shows the engineering stress-strain curve of magnesium alloy AZ91 and its composite reinforced with a different weight percentage of SiC particulates under tensile loading. The graphical bar charts representation of the ultimate tensile strength and yield strength are presented in Figure 5.9**.** The ultimate tensile strength (UTS) of magnesium alloy (AZ91) is found to be 187.6 MPa. The ultimate tensile strength of the 3% SiC particulate reinforced composite is lower than that of the magnesium alloy, and it increases with increasing the weight percentage of reinforcements. This result is in agreement with the investigation reported by Lou [211]. However, the ultimate tensile strength of 12% SiC particulate reinforced composite is higher than that of magnesium alloy AZ91.

The difference of ultimate tensile strength in AZ91 alloys and SiC particulates reinforced composite is due to its processing technique, which is stir casting in the present study. For the as-cast AZ91 composite ultimate tensile strength usually lower than that of as-cast AZ91 [211] because of the addition of any secondary hard phase particle and presence of porosity reduces tensile strength in the as-cast state. Further secondary processing such as extrusion, forging and rolling operation may have enhanced the properties due to the formation of the strong bond between reinforcement as well as the absence of microvoids and porosity in as-cast composites.

The yield strength of the composites observed to be increasing with the increase in weight percentage of SiC particles in magnesium alloy (AZ91) composites as depicted in Table 5.3 and Figure 5.9. The various strengthening mechanism can contribute to increased yield strength of the metal matrix composite, i.e. (a) Generation of geometrically necessary dislocation to accommodate thermal and elastic modulus mismatch between the matrix and reinforcement (b) Load- bearing effects due to the presence of reinforcement (c) Orowan strengthening (d) Hall- Petch effect due to grain size refinement. The detail discussion about different factors and mode of stress increment has already given in literature review, i.e., Chapter 2

Table 5. 3: The ultimate tensile strength and yield Strength

Materials	**UTS (MPa)**	**YS (MPa)**
AZ91	187.7	120.90
AZ91+3%SiC	112.6	72.61
AZ91+6%SiC	136.4	63.9
AZ91+9%SiC	139.5	96.34
AZ91+12%SiC	193.9	124.6

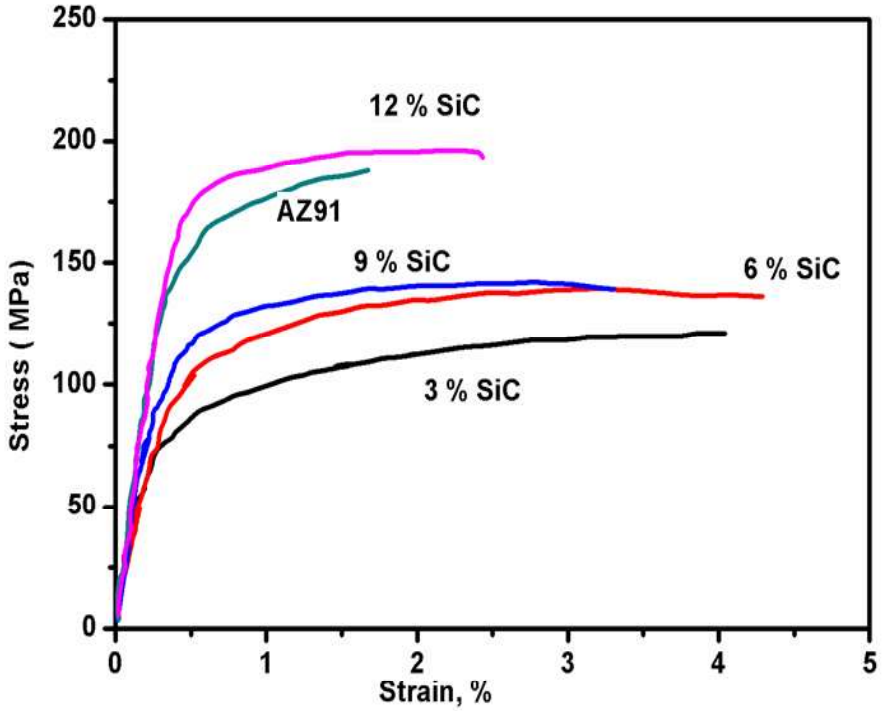

Figure 5. 8: Engineering stress-strain curve of AZ91 and its composite reinforced with SiC particulates

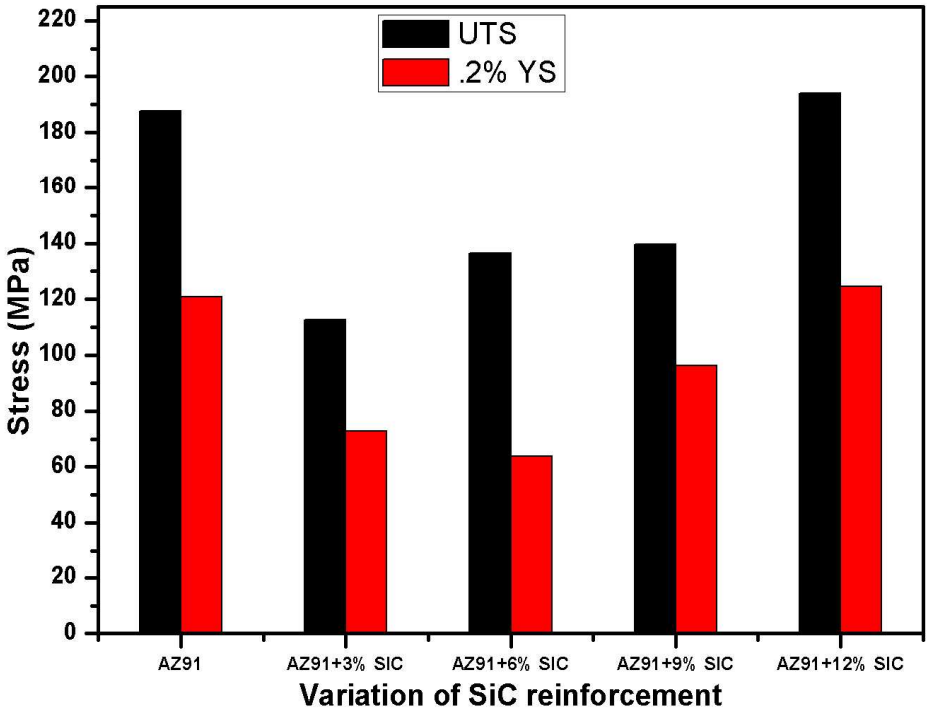

Figure 5. 9: Variation of ultimate tensile strength and yield strength with a variation of SiC particulates

5.2.6. Compressive test

The compression tests of AZ91 alloy and its composites have been performed, and the results are shown in Table 5.4. Figure 5.10 shows the graphical representation of the ultimate compressive strength in MPa. The ultimate compressive strength of the composite materials reinforced with SiC particulates is higher than that of unreinforced AZ91 magnesium alloy as depicted in Figure 5. 10. The ultimate compressive strength of the composite increased further as the weight percentage of SiC particulate increases in the base alloy AZ91. The ultimate compressive strength of the composites reinforced with different weight percent of SiC is increased because of the addition of hard particles in a softer matrix will increase load-bearing capacity. The effective load transfer is highly dependent upon the interfacial bonding between the matrix and the reinforcement. The significant improvements in ultimate compressive strengths are observed in the SiC particulate reinforced composites in comparison with monolithic alloy. The enhancement in ultimate compressive strength may be attributed due to the partial closure of the small microscopic cracks during compressive loading. A similar observation is also reported for SiC_p reinforced AZ92 magnesium alloy composites [212]. The Compressive strength is increased by 26.93% on addition of 3% of SiC particulate, and it further increased up to 49.41% on addition of 12 % of SiC particulate.

Table 5. 4: Ultimate Compressive strengths of AZ91 alloy and its composites

Materials	**Ultimate Compressive Strength (MPa)**
AZ91	308
AZ91+3%SiC	317
AZ91+6%SiC	323
AZ91+9%SiC	331.5
AZ91+12%SiC	342

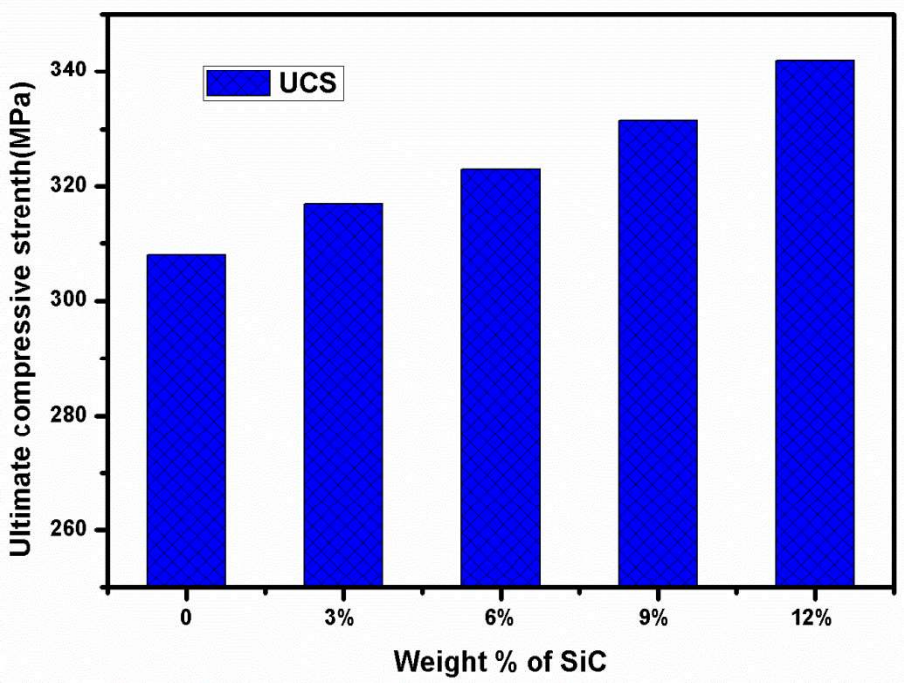

Figure 5. 10: Representation of ultimate compressive strength of alloy and composites with different percentage of SiC

5.2.7. Facto- graph of tensile and compressive tests

The fracture surfaces of the magnesium alloy AZ91 and as-cast composites reinforced with different weight percent (3, 6, 9 and 12 %) of SiC particulates were microscopically rough with a normal height variation of 2 mm. Figure 5.12 shows the SEM image of fracture surfaces of as-cast magnesium alloy AZ91 at different magnification. Figure 5.13 shows the SEM image of fracture surfaces of as-cast magnesium alloy AZ91 based composites reinforced with a different weight percentage of SiC particulates at different magnification. The main features of the fracture surface were locally concentrated SiC particles and agglomeration of SiC particles. De-bonding of the particle-matrix interface, cracks on the particles and inter-granular cracks in the matrix were also present. From the fracture surface investigation, it has been seen that fracture occurred via two types in the case of the composite. In the matrix phase, dominant regions ductile fracture of the matrix takes place in which void nucleation could play an important role.

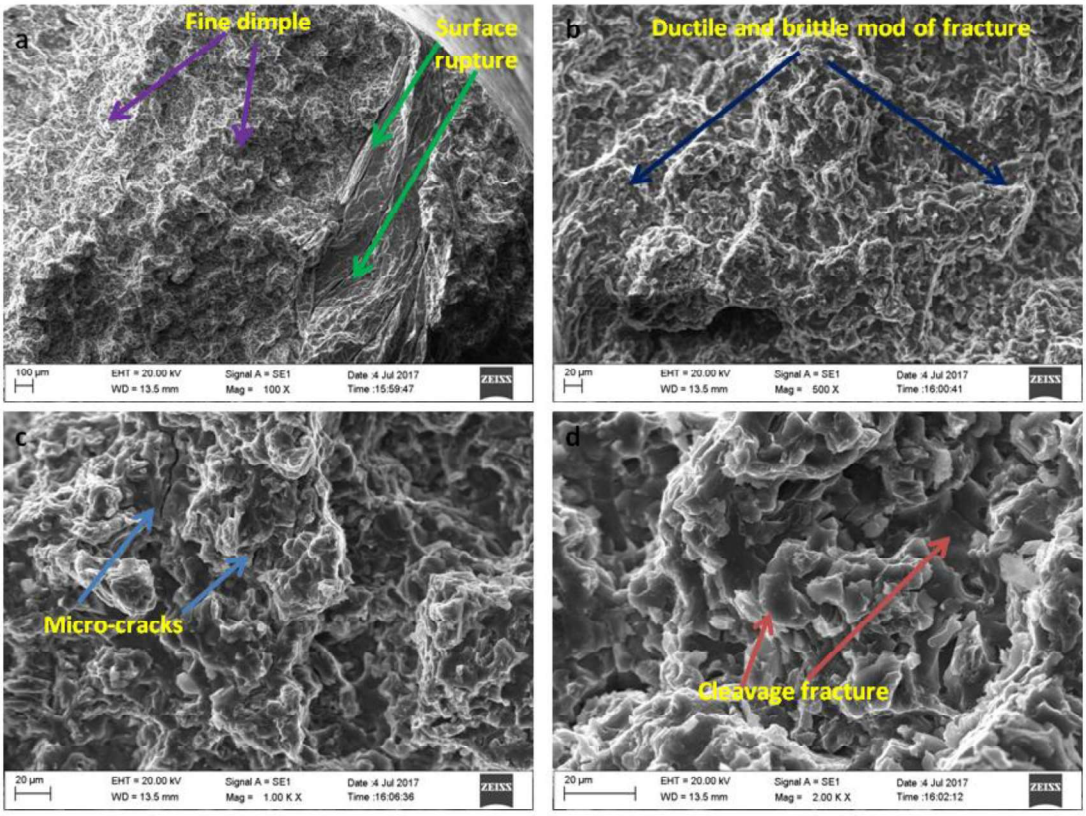

Figure 5. 11: SEM micrograph of cast magnesium alloy AZ91

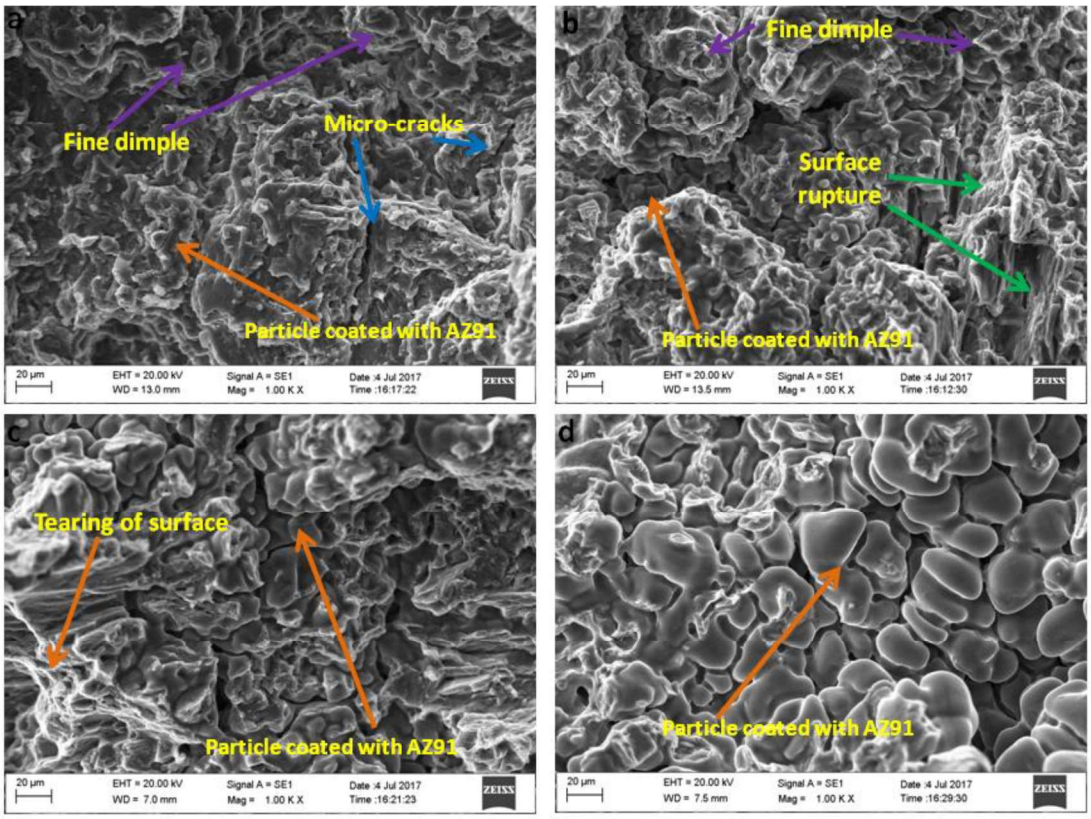

Figure 5. 12: SEM micrograph of cast magnesium alloy AZ91 based composites a) 3% SiC b) 6% SiC c) 9% SiC d) 12% SiC

The brittle fracture occurs where the concentration of the SiC particle is high. The composite tends to exhibit more brittle fracture morphology than the matrix alloy. The crack of the composite is started by de-bonding at the interface of the matrix and SiC reinforcement.

1. In the case of the matrix, the fracture occurs by cleavage mode, interspersed with the ductile feature.

2. The composite shows mixed mode fracture (i.e., ductile and cleavage), particle de-bonding is also observed.

3. The matrix particle interface would be predominantly governed by mechanical bonding, hence when the maximum load is reached rather than particle fracture de-bonding of SiC particulates occurs.

4. The fracture surface morphology of the composite also reveals that small size dimple, micro-crack, and cleavage fracture increases with increase in reinforcement.

In the compression test of AZ91 magnesium alloy and its composites, the fracture occurred nearly 45-degree angle concerning compression test axis and showed dominant shear failure.

Figure 5. 13: Fractured samples in a compression test

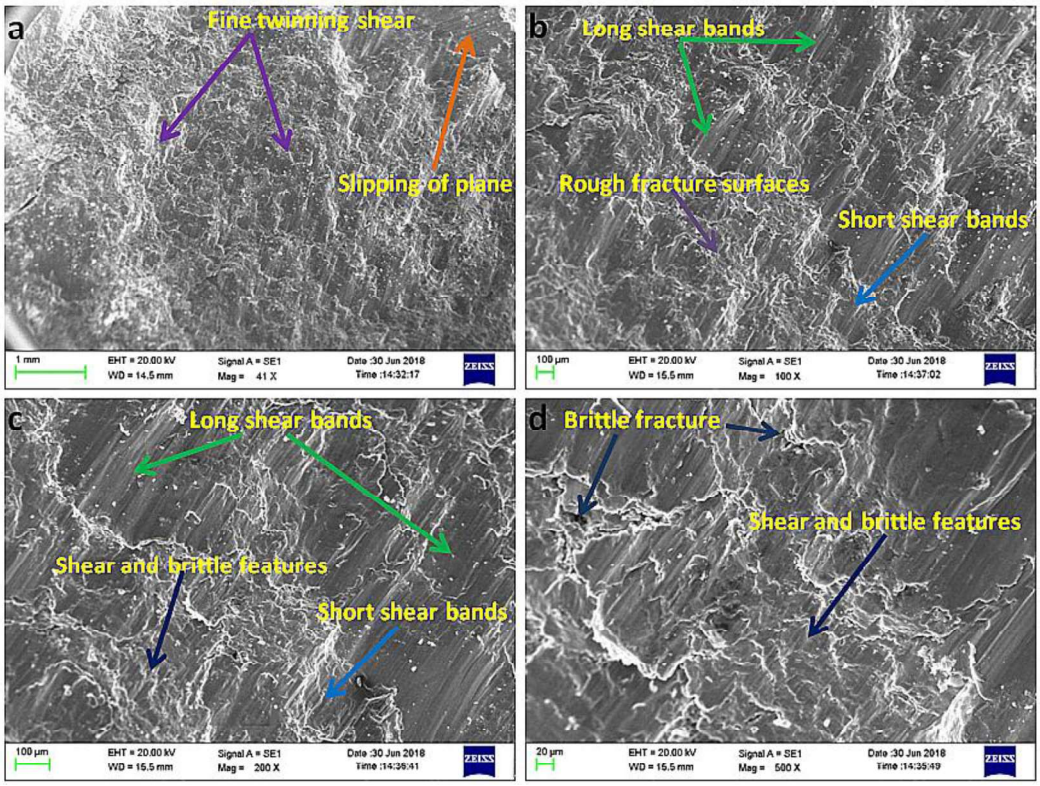

Figure 5. 14 SEM micrograph of the fracture surface of AZ91 at different magnification a) 41X b) 100X c) 200X d)500X

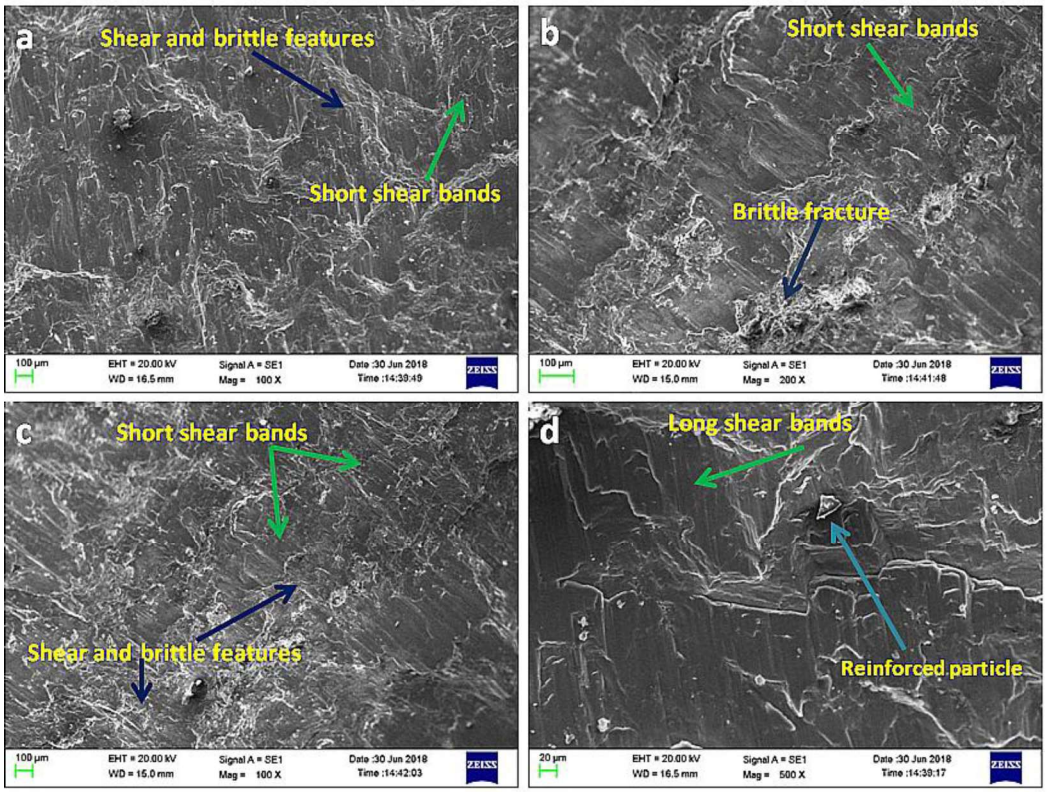

Figure 5. 15: SEM micrograph of fracture surface of AZ91 based composites reinforced with a) 3% SiC b) 6% SiC c) 9% SiC d) 12% SiC

Figure 5.14 shows the micrograph of compressive fracture surfaces of AZ91 magnesium alloy and its composites. Figure 5.15 shows the SEM micrograph of the fracture surface of AZ91 at different magnification, i.e., 41X, 100X, 200X and 500X. Figure 5.16 shows the SEM micrograph of the magnesium alloy AZ91 based composites reinforced with a different weight percentage of SiC particulates. The fracture surface of AZ91 exhibit dominant shear failure and showed more shear bands when compared to AZ91 / SiC composites, which on the other hand shows rough fracture surfaces with a mixed mode of shear and brittle features. Short and long shear bonds are seen in the fracture surfaces along with the shear twinning mode of plastic deformation. The rough, brittle and shear mode is the common fracture mode in magnesium alloys and its composites.

5.2.8. Pin on Disk Sliding Wear Test

The process of material removal from the one or both of two solid mating surfaces is called wear. It is a solid state surface phenomenon and occurs mostly at outer surfaces of the contacting bodies. The materials with the modified surface are better than wear resistant material. Pin on disk friction and wear testing machine is used to evaluate the tribological characteristics of the magnesium alloy and its composites with different percentage of SiC particulates. The wear sample is made as per ASTM standard: G99. The friction wear weight losses are generated by varying the normal load at two different velocities for all the composites.

Fabricated AZ91 alloy based metal matrix composite materials in this work are expected to offer some benefits for tribological applications, where materials with lower density are desired. The specimens are weighed before and after the test using a balance having an accuracy of 0.0001 g to measure the weight loss. The wear rates are

calculated from the volume loss divided by sliding distance. The data for the wear tests are taken from the average of the three measurements. The worn surfaces are observed using the scanning electron microscopy (SEM) and before that the worn surfaces are cleaned thoroughly to remove the wear debris.

a) Dry sliding test parameter and wear behavior

The dry sliding wear test for AZ91 alloy and its composite with the different percentage (3, 6 9 and 12) of SiC_p has been performed. The variations of sample weight loss with constant sliding speed are observed under variable normal load from 9.81 N (1 kgf) to 58.86 N (6 kgf). The different parameter used in dry sliding wear test are tabulated in Table 5.5

Table 5. 5: Parameters for the pin on disk dry sliding wear test

Sr. No	**Parameters**	**Value/ description**
1.	**Pin materials**	AZ91 and its composite reinforced with SiC (3%, 6%, 9%, and 12%)
2.	**The dimension of the Pin**	30 mm length and 8 mm in diameter
3.	**Disk Material**	Tool steel grade EN31
4.	**Track diameter (D)**	83 mm for all experiments
5.	**Load Variation (N)**	9.81 N, 19.62 N, 29.43 N, 39.24 N, 49.05 N, 58.86 N (for RPM-320)
		19.62 N, 39.24 N, 58.86 N (for RPM-600)
6.	**Sliding Time (t)**	15 minutes
7.	**Speed Variation (n)**	320 RPM and 600 RPM

The formula used for calculation of sliding velocity (v) and sliding distance (l) is given below:

$$v = \frac{\pi Dn}{60000} m/s \qquad (5.1)$$

and

$$l = \frac{\pi Dnt}{60} mm \qquad (5.2)$$

Where D is the track diameter (mm), n is the revolution speed (RPM), and t is the sliding time (second).

The wear weight loss of AZ91 alloys and SiC_p reinforced composite were plotted against different normal loads at the constant sliding speed of 1.39 m/s in Figure 5.16. The wear weight loss of unreinforced magnesium alloy having a higher value than composites at all the normal load for sliding speed of 1.39 m/s as seen in Figure 5.16. As the percentage of reinforcement increases in the composite, the wear weight loss decreases for all the different (3, 6, 9 and 12) percentage of the SiC particulates reinforcements. However weight loss for the composite increases with an increase in normal load. The estimation of wear weight or wear volume may be estimated by Archard's law [161]. According to Archard's law material loss in wear is directly proportional to sliding distance and normal applied load but indirectly proportional to material hardness. The Archard's law is applicable mainly for single phase materials, but it works fairly for multiphase alloys and composites. This law is proposed only for adhesion wear. Therefore the composite materials are observed to be slightly less severe than monolithic alloys. The composite materials having higher hardness than unreinforced alloy due to the addition of hard SiC particulate favor less wear as per Archard's law (wear rate is inversely proportioned to the hardness). The Archard law can be written as

$$V = K_1 N l / 3H \qquad (5.3)$$

Where, V is the volume loss in wear, N is the normal applied load, l is the sliding distance and H is the hardness of the test materials. K_1 is wear constant that depends on elastic plastic contacts, shearing of those contacts, effect of environment, mode of

lubrication, etc. The adhesive wear is generally associated with low normal load and low sliding velocity. The others wear mechanisms also involved in the material removal process of dry sliding wear.

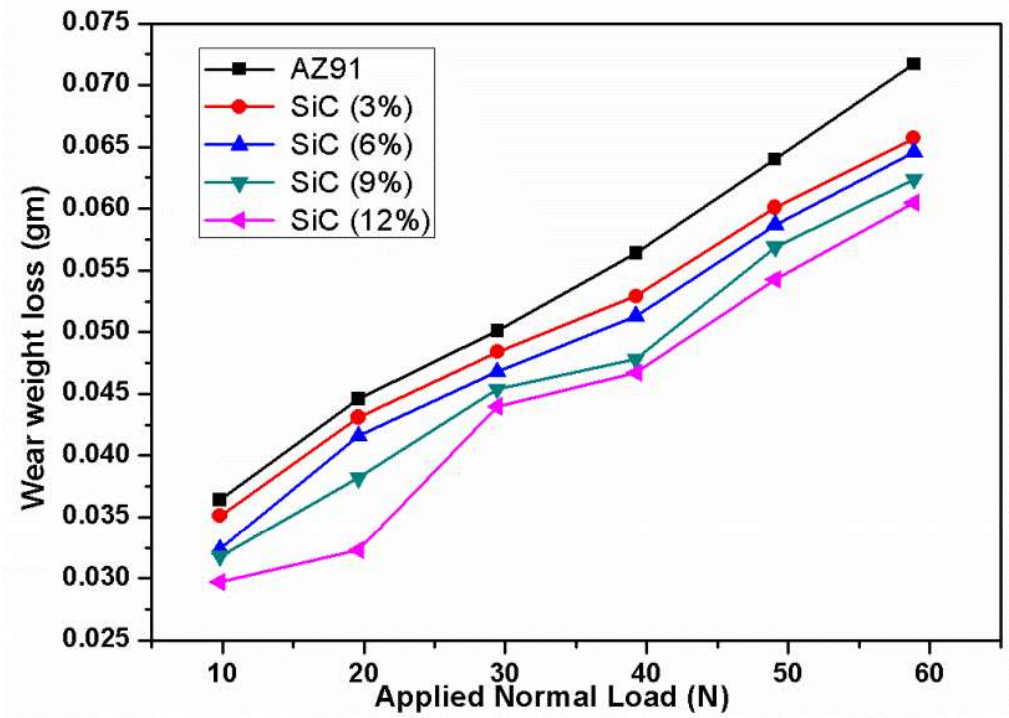

Figure 5. 16: The variation of wear weight loss with normal load at a constant sliding speed of 1.39 m/s

The combined effect of different wear mechanism involved in the estimation of wear loss. The addition of hard particle (SiC) in base alloy AZ91 may provide dry lubrication, and it can provide rolling contact between the hard disk materials and soft pin materials. Therefore on increasing the amount of reinforcement, the wear weight loss and wear volume decrease in the case of particulates reinforced composites. Figure 5.17 shows the wear rate (mm^3/m) at different normal load. It seems that wear rate is greater at the higher load and the wear rate decreased on increasing the weight percentage of SiC particulate reinforcement. The wear rate plot concerning applied normal load is almost linear which is in conforming to the Archard's law. The variations of the average sliding coefficient of friction (μ) with a different value of applied normal

loads are shown in Figure 5.18. The average coefficient of friction decreases as the normal load increases in all the cases, irrespective of alloy and composite. The average coefficient of friction value at lower load is slightly different from its behaviors at higher loads. The unreinforced alloy has a higher value of the coefficient of friction than SiC particulate reinforced composite. The decrease in the average coefficient of friction with an increase in normal applied load has been reported by YANG and CHUNG earlier [213]. However, the extent of decrease is to be correlated with types, size, and distribution of reinforcements. Figure 5.19 shows the average sliding coefficient of friction (μ) with different percentage of SiC particulate reinforcements. It is clear from Figure 5.19 that the coefficient of friction for magnesium alloy and its composites at lower load is higher, but it is lower at higher load. The small variation in coefficient of friction is observed in composites at higher load and a higher percentage of reinforcements. This behavior can be explained with the phenomenon that on increasing applied normal load the asperities of the mating surfaces will be deformed, and this will lead to a decrease in coefficient of frictions. The wear rates at two different speeds concerning three different loads are presented in Figure 5.20 to Figure 5.24 for the monolithic alloy, and it composites reinforced with different percentage of SiC particulates. It can be concluded from the Figure 5.20 to Figure 5.24 that the wear rates at the sliding speed of 2.60 m/s are higher than the wear rates at the sliding speed of 1.39 m/s irrespective of base alloy and composites. The difference in wear rates at these two velocities (1.39 m/s and 2.60 m/s) is highest in case of base alloy AZ91. However, in the case of composites, this difference decreases as the percentage of reinforcement increases.

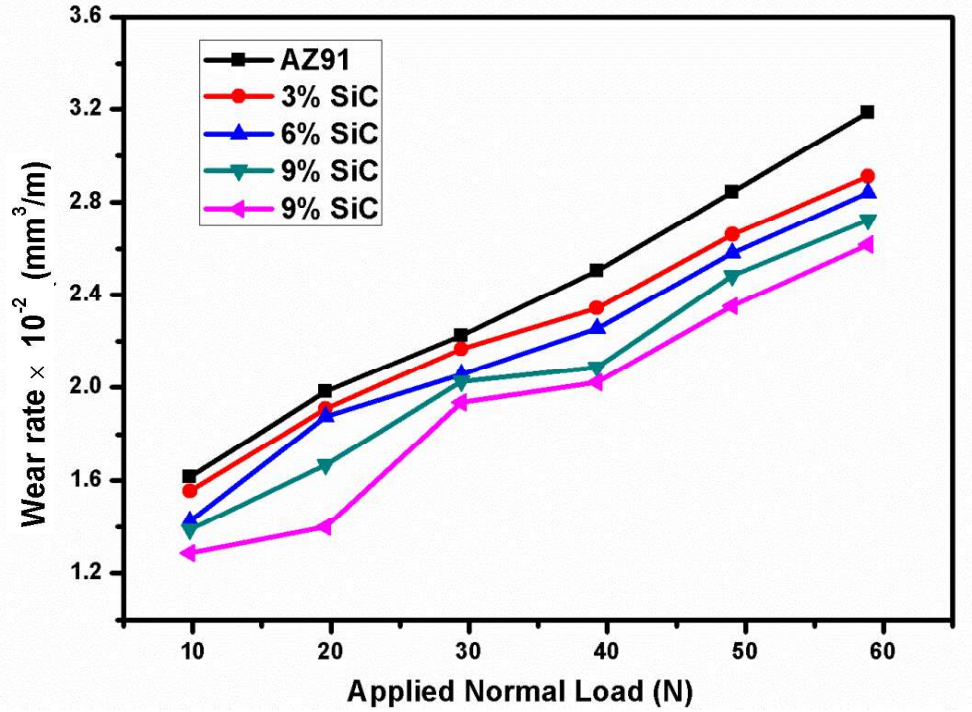

Figure 5. 17: The variation of wear rate with an applied normal load of AZ91 magnesium alloy and its composite reinforced by SiC particulates

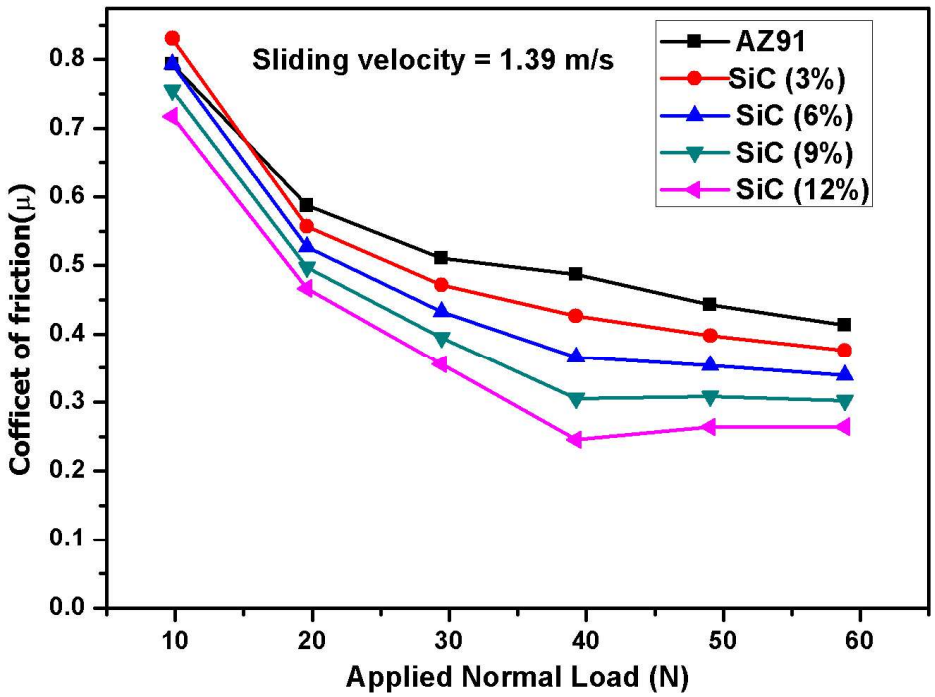

Figure 5. 18: Average coefficient of friction of the AZ91 magnesium alloy and its composites at different normal load

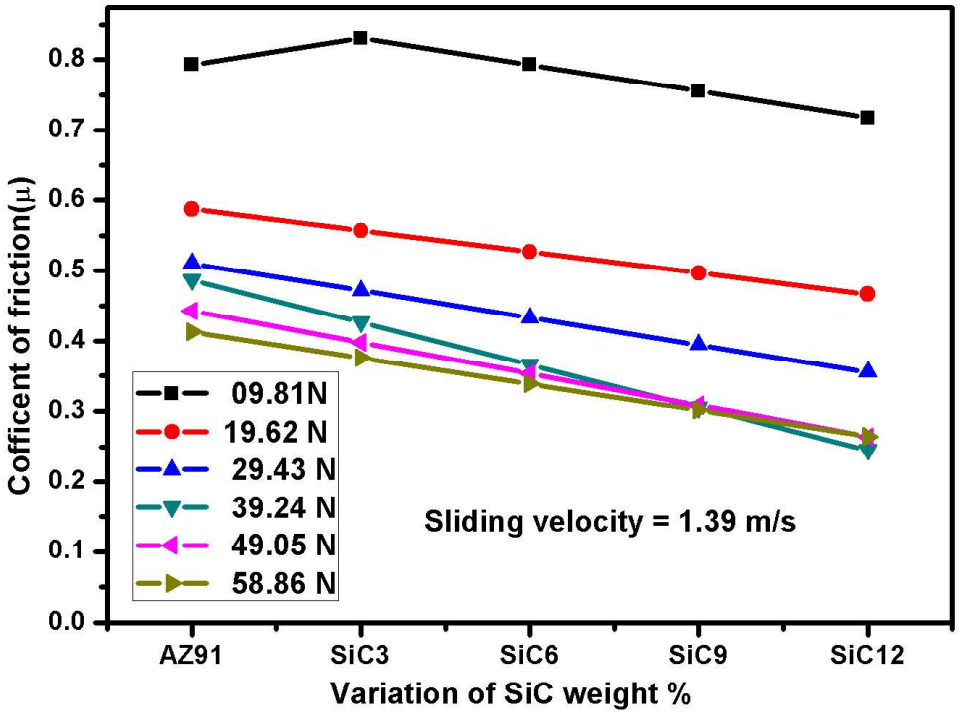

Figure 5. 19: Variation average coefficient of friction of the AZ91 magnesium alloy and its composites at a different weight percentage of SiC and different normal load

The wear rate of magnesium alloy and composites is a function of sliding velocity, normal load, and environmental conditions. The variation of wear rate at different velocity and load is due to the presence of different wear mechanisms, which may be a very complex phenomenon to understand. The wear rate at a velocity lower than 1 m/s is different from the wear rate at a velocity higher than 1 m/s as reported by Lim et al. [162]. A similar trend is also observed in current research that on increasing velocity or load the wear rate is generally increases. This can be observed in graph plotted from Figure 5.21 to Figure 5.25.

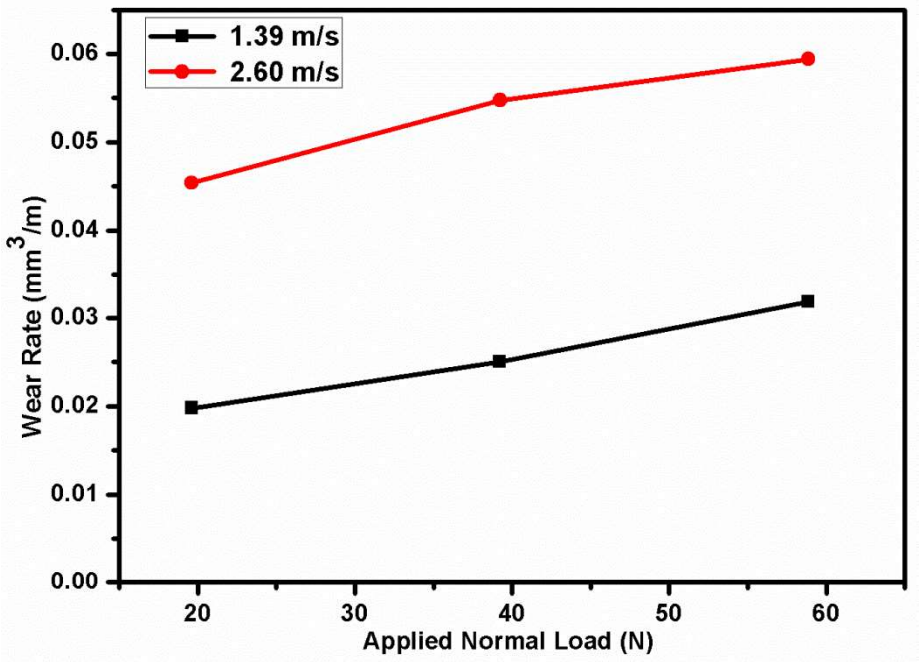

Figure 5. 20: Variation of wear loss of AZ91 magnesium alloy at different velocity and different applied normal load

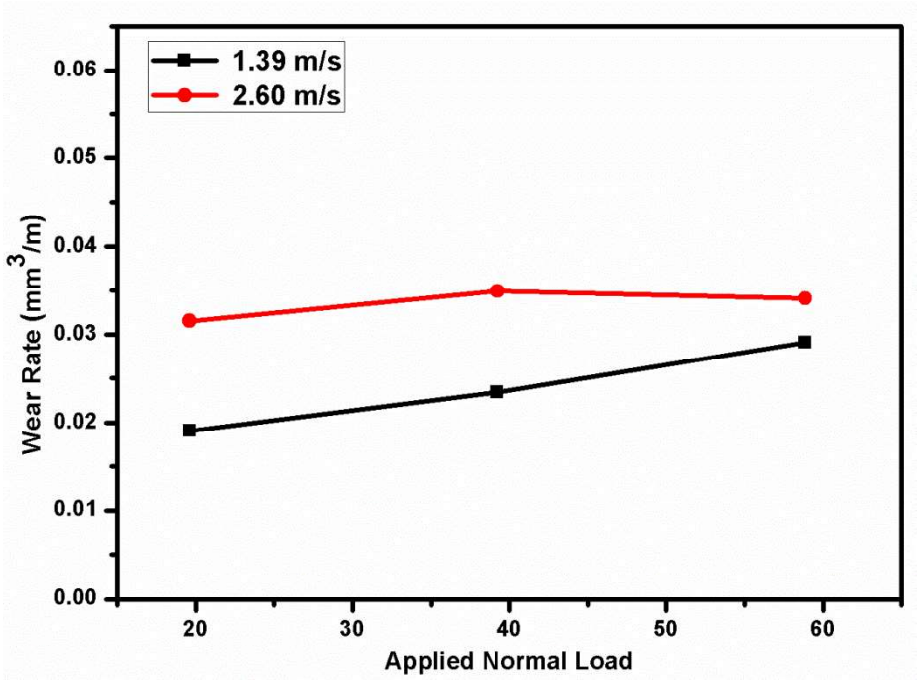

Figure 5. 21: Variation of wear loss of 3 weight percent SiC in AZ91 magnesium alloy at different velocity and different applied normal load

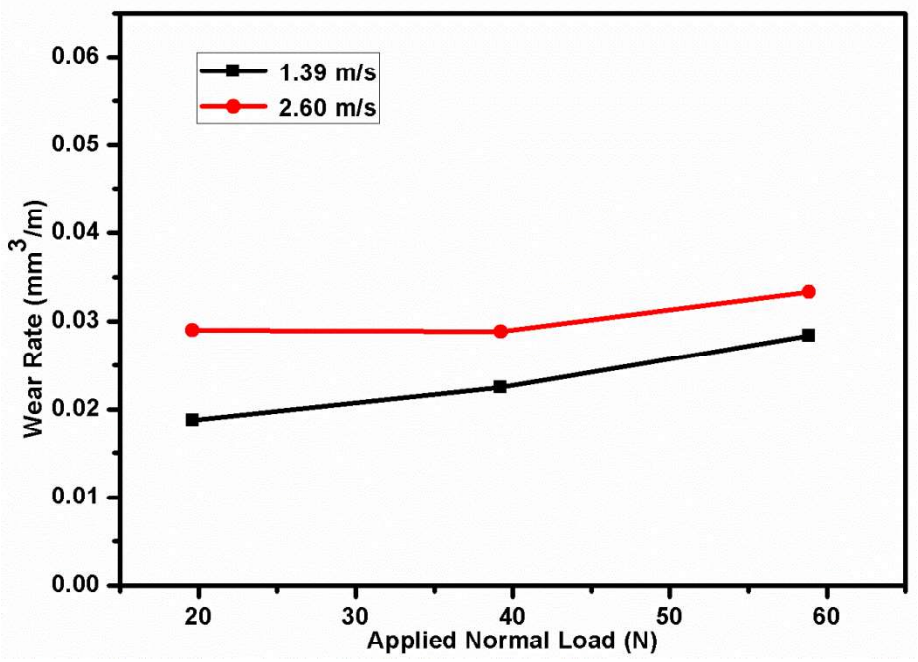

Figure 5. 22: Variation of wear loss of 6 weight percent SiC in AZ91 magnesium alloy at different velocity and different applied normal load

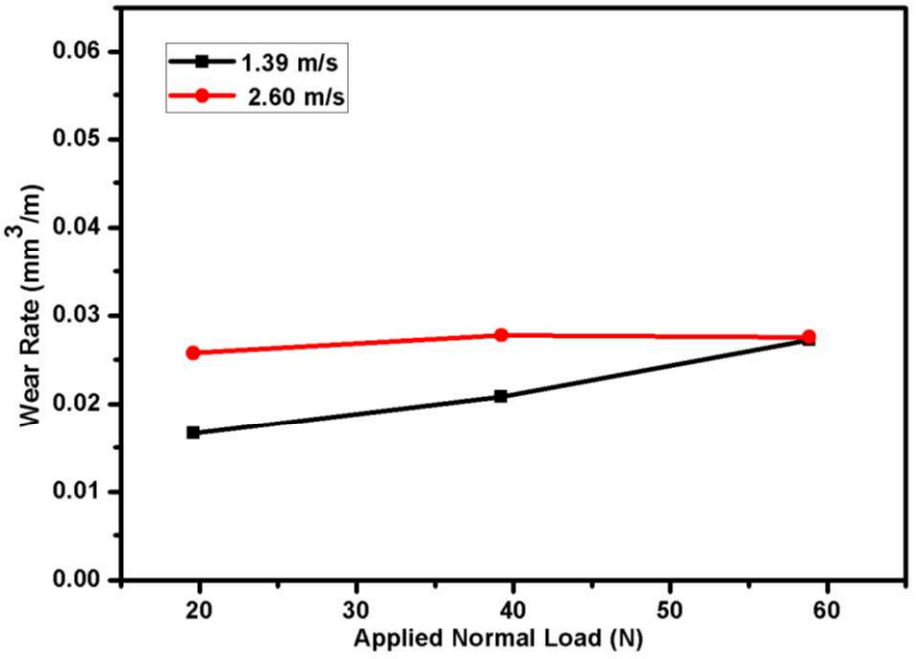

Figure 5. 23: Variation of wear loss of 9 weight percent SiC in AZ91 magnesium alloy at different velocity and different applied normal load

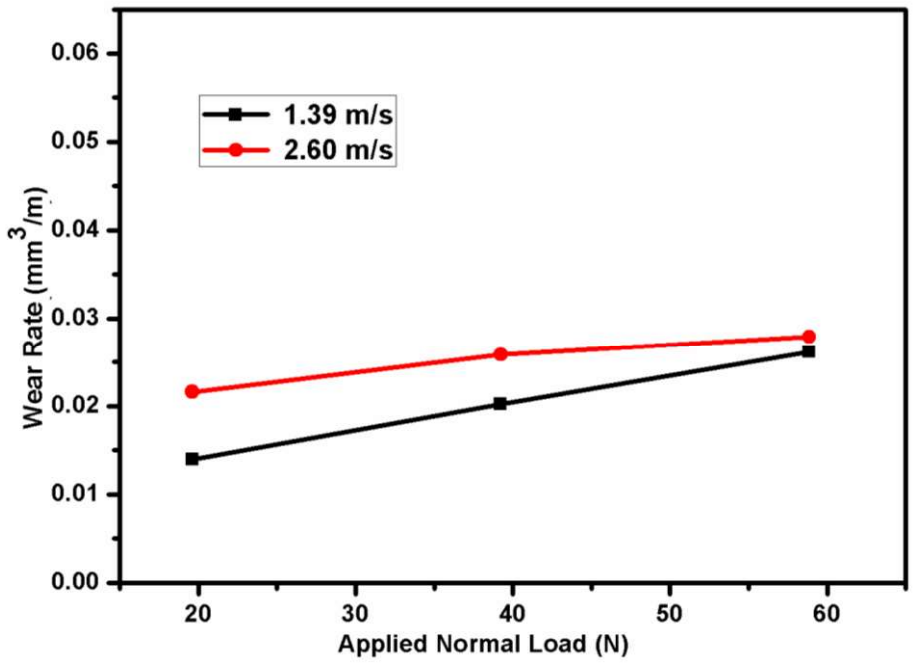

Figure 5. 24: Variation of wear loss of 12 weight percent SiC in AZ91 magnesium alloy at different velocity and different applied normal load

b) Examination of sliding surfaces and Wear mechanism

The worn pin surfaces are examined by scanning electron microscope to predict the different wear mechanism occurred during sliding on the hard disk in pin on disk dry sliding wear test. Figure 5.25 shows the selective SEM micrograph of worn surfaces of the magnesium alloy AZ91 at different load, velocity and magnifications. Several grooves and scratches are present on almost all the worn pin within this velocity and load range. The oxidation wear was observed at low velocity lower normal load. Figure 5.26 shows the selective SEM micrograph of SiC reinforced AZ91 magnesium alloy composites at different load, velocity and weight percentage of reinforcements. In the case of composite plowing delamination and oxidation, wear are prominently present in the worn surfaces. A large amount of accumulated embedded debris is also observed at the worn surfaces of the pin. The energy dispersive X-ray spectroscopy (Figure 5.27) identified stronger peaks of oxygen than Al and Zn, which indicate the presence of

magnesium oxide in the wear debris. This behavior is indicative of oxidative wear, which is developed due to frictional and sliding heating of the pin materials. Composite materials exhibit the extensive formation of oxide than unreinforced magnesium alloy. Five different wear mechanism may be operated singly or in combination under different normal load and sliding speed. The wear mechanism may be abrasion, oxidation, delaminating, adhesion and thermal softening and melting. It is very difficult to examine the exact influence of one or others wear mechanism correctly. The wear behavior within this velocity is oxidation at lower load and de-lamination or abrasion wear at higher load. Several grooves and scratch marks parallel to the sliding direction is evidence of abrasion wear. The de-attachment of wear particle occurs in the form of sheet and short cracks roughly perpendicular to the sliding direction. This type of wear mechanism is classified as delamination wear, and it was first introduced by N.P Suh [144]. The oxidation wear also occurred under the test conditions and due to oxidation material surface become dark at the wear surfaces.

A summary of different wear mechanism for a different combination of sliding velocity and applied normal load is predicted in Table 5.6. Pins tested at load 19.62 N and 2.6 m/s exhibit series of short cracks nearly perpendicular to the sliding direction. The cracks removed in the form of small broken sheet and flakes is suggested as delamination wear by several researchers [162], [214], [215].

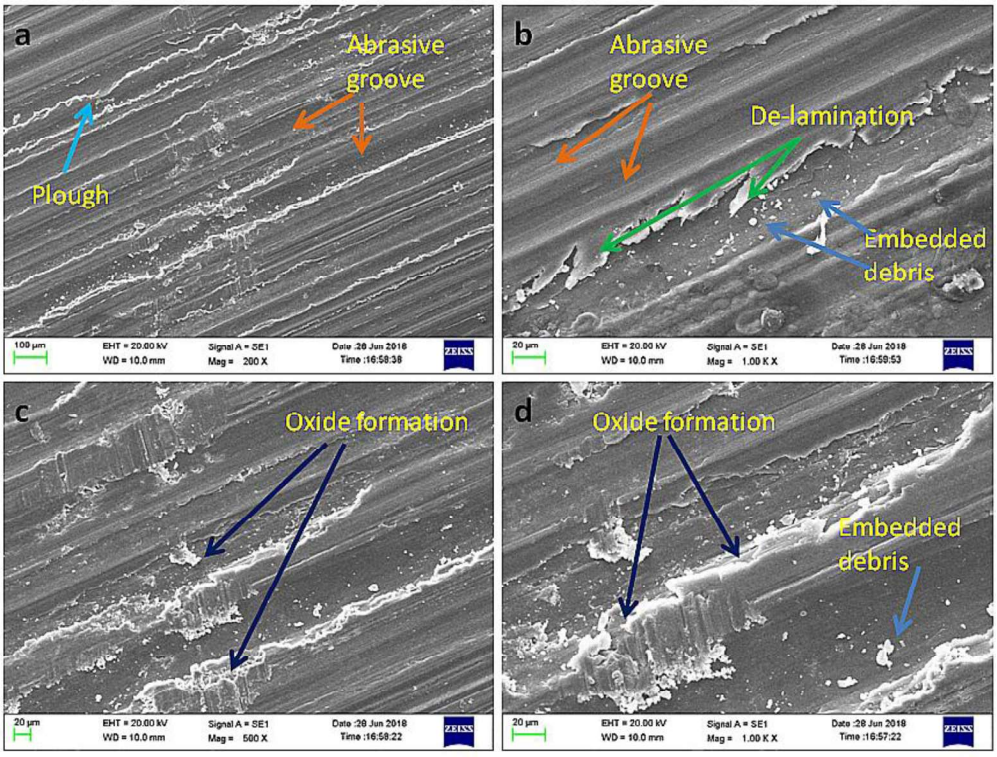

Figure 5. 25: SEM micrographs of the worn surfaces of AZ91 magnesium alloy a) 39.24 N, 2.6 m/s and 200X b) 19.62 N, 2.6 m/s and 1000X c) 39.24 N, 1.39 m/s and 500X d) 39.24 N, 1.39 m/s and 1000X

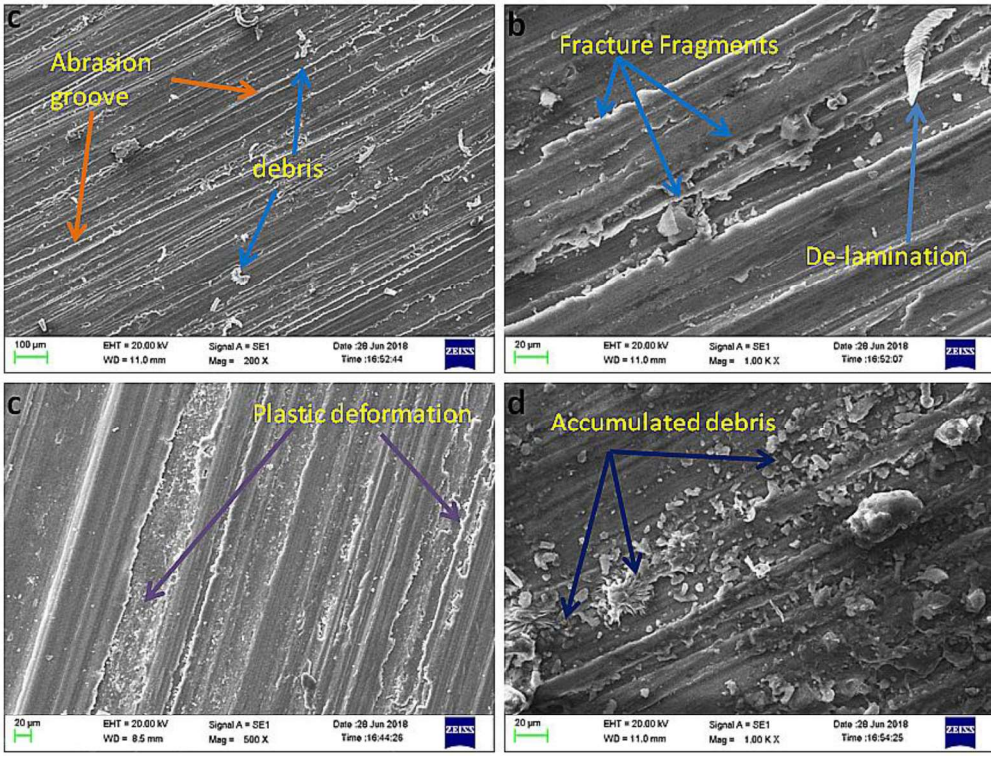

Figure 5. 26: SEM micrographs of the worn surfaces of SiC reinforced AZ91 magnesium alloy composite a) 39.24 N, 1.3 m/s and 6% SiC b) 19.62 N, 2.6 m/s 3% SiC c) 58.86 , 2.6 m/s 9% SiC d) 39.24 N, 2.6 m/s 12% SiC

Table 5. 6: Summary of wear mechanisms for different combination of normal load, sliding speed and pin materials

Load (N)	Sliding speed (m/s)	Pin material	Wear Mechanism				
			Abrasion	Oxidation	Delamination	Adhesion	Softening/ melting
19.62	1.39	AZ91	*	**	**		
		AZ91+3% SiC	*	**	**		
		AZ91+6% SiC	*	**	**		
		AZ91+9% SiC	*	**	**		
		AZ91+12% SiC	*	**	**		
19.62	2.6	AZ91	*	*	**	*	
		AZ91+3% SiC	*	*	**	*	
		AZ91+6% SiC	*	*	**	*	
		AZ91+9% SiC	*	*	**	*	
		AZ91+12% SiC	*	*	**	*	
39.24	1.39	AZ91	**	**	*	**	
		AZ91+3% SiC	**	**	*	**	
		AZ91+6% SiC	**	**	*	**	
		AZ91+9% SiC	**	**	*	**	
		AZ91+12% SiC	**	**	*	**	
39.24	2.6	AZ91	**	*	*	**	
		AZ91+3% SiC	**	*	*	**	
		AZ91+6% SiC	**	*	*	**	
		AZ91+9% SiC	**	*	*	**	
		AZ91+12% SiC	**	*	*	**	
58.86	1.39	AZ91	*			***	
		AZ91+3% SiC	*			***	
		AZ91+6% SiC	*			***	
		AZ91+9% SiC	*			***	
		AZ91+12% SiC	*			***	*
58.86	2.6	AZ91	*			***	*
		AZ91+3% SiC	*			***	*
		AZ91+6% SiC	*			***	*
		AZ91+9% SiC	*			***	*
		AZ91+12% SiC	*			***	*

The relative predicted the extent of each wear mechanism: * slight; ** Moderate; *** heavy

At higher speed 2.60 and higher load 58.86 N the oxidation and delamination are wholly converted into adhesion wear. Due to higher load and velocity pin materials become soft; there are also sign of plastic deformation and smearing. The region of

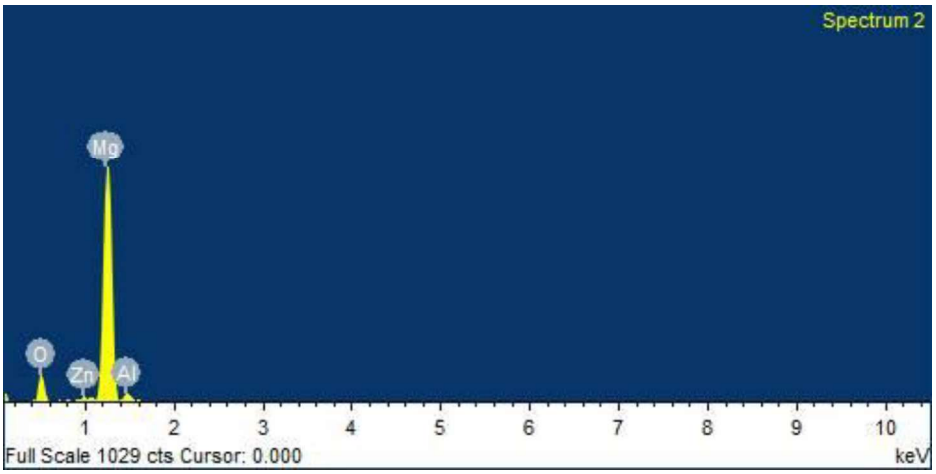

Figure 5. 27: Energy-dispersive X-ray spectroscopy of worn surfaces

The dominance of the wear mechanism depends on the normal load and sliding speed. Abrasion, oxidation, and delamination wear mechanism are generally dominant in lower sliding velocity and lower load region while adhesion and thermal softening/ melting are dominant in higher sliding velocity and loads.

5.3. Conclusions

The following conclusion that can be drawn from this chapter:

1. The addition of a small percentage of the hard ceramic particle (SiC_p) led to refined the microstructure of the magnesium alloys based metal matrix composites.
2. The density and porosity of the magnesium alloy based composites are increased with increase in wt % of SiC particulates.
3. The XRD results from peaks confirm the presence of Mg, $Mg_{17}Al_{12}$ and SiC Phases.
4. The Vickers microhardness value is increased by ~ 30% on addition of 3% of SiC particleses, and it is further increased up to ~78% on addition of 12 % of SiC particulates.

5. The tensile strength was found to initially decrease and then increase with the increase in the SiC particulates in magnesium alloys.
6. The Compressive strength is increased by ~27% on addition of 3% of SiC particulate, and it is further increased up to ~50% on addition of 12 % of SiC particulate.
7. The composite materials show the mixed mode fracture (i.e., ductile and cleavage). The fracture surface morphology of the composite also reveals that small size dimple, micro-crack, and cleavage fracture increases with increase in reinforcement.
8. The compression fracture surface of AZ91 exhibit dominant shear failure and showed more shear bands when compared to AZ91 / SiC composites, which on the other hand shows rough fracture surfaces with a mixed mode of shear and brittle features.
9. The wear weight loss and wear rate of the SiC reinforced composites is lower than the unreinforced composites.
10. The average coefficient of friction of the composite is lower than that of unreinforced alloy, and it is decreased with an increase in normal load.
11. The wear rate at higher sliding velocity is higher, and the effect of differences in velocity is decreased with the increase in normal loads.